Imaging the Thermodynamic State of Lipid Membranes with Multiplex CARS Microscopy

Michiel Müller* and Juleon M. Schins

Swammerdam Institute for Life Sciences, University of Amsterdam, P.O. Box 94062, 1090 GB Amsterdam, The Netherlands

Received: October 31, 2001; In Final Form: January 8, 2002

Multiplex coherent anti-Stokes Raman scattering (CARS) microscopic imaging is demonstrated for the first time and used to visualize the thermodynamic state, either liquid crystalline or gel phase, of lipid membranes. Whereas in spontaneous Raman scattering the low scattering cross section is generally prohibitive for high-resolution microscopic imaging, the signal enhancement in multiplex CARS, by more than 4 orders of magnitude, enables microscopic imaging with realistic frame rates ($\sim$min^{-1}). Because of the broad spectral window over which the CARS signal is detected simultaneously, the identification of the thermodynamic state of the lipid membranes can be accomplished directly, without any additional tuning of the lasers. We demonstrate that the experimental CARS spectral data are highly consistent with those obtained with spontaneous Raman scattering, with a signal-to-noise ratio determined only by Poisson noise. In addition, the inherent intensity normalization renders multiplex CARS a robust imaging technique.

Introduction

Raman spectroscopy is sensitive to molecular vibrations, which in turn reflect inter- and intramolecular interactions. As such, Raman spectroscopy is unique in that it provides detailed molecular information and specificity at room temperature, even within extremely complex systems such as living cells.[1] Particularly attractive to the application of Raman spectroscopy to microscopy is the fact that the contrast of the image is based on the inherent molecular properties of the specimen and does not require the use of specific labels (as in fluorescence microscopy). However, Raman spectroscopy suffers especially from a low scattering cross section as well as from interference from naturally occurring luminescence. These aspects are generally prohibitive for the application of spontaneous Raman scattering to high-resolution (3-D) microscopy.

CARS, coherent anti-Stokes Raman scattering, is a nonlinear optical analogue of spontaneous Raman scattering. In this technique, a particular Raman transition is coherently driven by two laser fields and subsequently probed by a third laser field generating an anti-Stokes signal field. The coherent nature of the process provides an orders-of-magnitude increase in signal strength (compared to that of spontaneous Raman scattering), permitting its use in high-resolution microscopy with typical image acquisition times on the order of minutes. In addition, the anti-Stokes signal is coherently emitted in the forward direction with a shorter wavelength than that of the excitation laser fields, making it readily separable from luminescence from the specimen and easy to collect. When the lasers are tuned far away from one-photon resonances, no net energy transfer to the specimen results from the interaction, which renders CARS microscopy a potentially mild, nondisruptive imaging technique for biological applications and also guarantees the absence of the fading of contrast, which can be a severe problem in fluorescence-based techniques. CARS microscopy was first experimentally demonstrated by Duncan et al.[2] and has recently been further developed by several groups.[3−7] In all of these applications, a single vibrational mode within the sample was selected by tuning the frequency difference between the two excitation laser fields to a particular vibrational resonance. The imaging of other vibrational modes in these "narrow-band" CARS configurations required additional tuning of one of the lasers.

In this contribution, we report on the application of multiplex CARS to high-resolution 3-D microscopy. In multiplex CARS, a significant spectral range of vibrational resonances is addressed simultaneously. Thus, in multiplex CARS, a complete CARS spectral window is acquired concurrently instead of a point-by-point acquisition of the CARS spectrum by subsequent tuning of one of the lasers, as in narrow-band CARS. This approach is particularly advantageous for the identification of the chemical constituents or the physical state of the sample and has been used widely in various spectroscopic applications (see refs 8, 9). In general, a single point in the CARS spectrum is insufficient for this purpose; it requires analysis of a spectral band (line shape, relative peak heights of multiple vibrational modes, etc.). Resolving spectral features in narrow-band CARS is limited by signal strength fluctuations that result from fluctuations in laser pulse energy, pulse width, timing jitter between the laser and Stokes pulses, etc. In multiplex CARS, the complete spectral band is recorded simultaneously, eliminating sources of noise induced by laser stability. In addition, this insensitivity to power fluctuations increases the possible detection sensitivity of the technique to the point that it is limited only by Poisson noise. Finally, the use of a significant CARS spectral window helps, in practice, to identify possible contamination of the sample and artifacts and aids in the in situ determination of the magnitude of the nonresonant background, all of which are more complicated in narrow-band CARS.

To achieve high spectral resolution, multiplex CARS requires a combination of a narrow- and a broad-band laser. The narrow-band laser determines the inherent spectral resolution of the

* To whom correspondence should be adressed. E-mail: muller@science.uva.nl. Tel: 31-20-5256221. Fax: 31-20-5256271.

10.1021/jp014012y CCC: $22.00
Published on Web 03/15/2002

measurement, and the broad-band laser determines the spectral width of the generated CARS spectrum. Typical Raman spectral features in biology have a width >7 cm^{-1}, thus our 1.5 cm^{-1} narrow-band laser (corresponding to ~10 ps) provides ample spectral resolution. For the broad-band laser, a compromise has to be found between spectral width and CARS signal strength because the magnitude of the CARS signal from a particular spectral feature decreases linearly with the spectral bandwidth of the broad-band laser. In the experiments reported here, an ~180 cm^{-1} broad-band laser source was used. This bandwidth corresponds to an ~80 fs transform limited pulse.

There is accumulating evidence that the biological function of the lipid membranes of cells is regulated by the lipid chemical composition and physical structure. In particular, high phase-transition lipids in combination with cholesterol are assumed to associate in domains (so-called lipid rafts), which are assumed to have an important function in signal transduction at the plasma membrane during intracellular sorting of proteins and lipids as well as during membrane fission (see refs 10−12). As a possible mechanism, it has been suggested that the formation of these lipid domains results from a phase separation between a liquid-ordered and a liquid-disordered phase.[13] So far, however, experiments have had to rely on indirect biochemical methods (such as detergent solubility) or the use of fluorescent markers[14]. CARS microscopy has the potential to address these issues directly. As a first demonstration of the principles and application of multiplex CARS to high resolution 3-D microscopy, we chose to image simplified model systems (multilamellar lipid vesicles) on the basis of their thermodynamic states. In particular, we address the response of these systems in the skeletal optical mode frequency range of the Raman spectrum, which is highly informative on lipid acyl chain interactions while being quite insensitive to the particular chemical structure of the lipids. Using both liquid crystalline and gel-phase multi-lamellar lipid vesicles, we demonstrate that experiment and theory of both spontaneous Raman scattering and CARS yield an internally consistent data set, which readily permits discrimination between the two thermodynamic states of the vesicles.

Experimental Section

Multiplex CARS. In multiplex CARS, a significant range of vibrational frequencies is addressed simultaneously by using a combination of a narrow- and a broad-band lasers. The two laser beams, denoted by *Laser* (frequency ω_L) and *Stokes* (ω_S) in the following, set up a grating off of which the *Laser* undergoes a Bragg diffraction, generating a broad-band−anti-Stokes signal beam at frequency $\omega_{AS} = 2\omega_L - \omega_S$ (see Figure 1a). The anti-Stokes signal is significantly enhanced when the frequency difference between *Laser* and *Stokes* matches a vibrational mode in the sample ($\omega_L - \omega_S = \omega_{vib}$). The bandwidth of the anti-Stokes signal is determined by the *Stokes* spectral-intensity profile, whereas the inherent spectral resolution is determined by the *Laser*. As is the case for all so-called parametric processes, no energy is deposited onto the sample to generate the anti-Stokes photon.

CARS Microscope. The layout of the multiplex CARS microscope is schematically depicted in Figure 2. It is based on a colinear phase-matching configuration of *Laser* and *Stokes*, which are synchronized in time and focused by a high numerical aperture (1.25 NA/63x oil immersion) microscope objective (O_1) onto the sample. The CARS signal is collected in the forward direction with a second microscope objective (1.25 NA/100x oil immersion; O_2) and then passes a holographic SuperNotch-Plus filter (F_1) with an optical density at 710 nm of = 6.0 and a spectral bandwidth of 280 cm^{-1} (Kaiser Optical Systems, Inc., Ann Arbor, MI) and a short-wave pass filter with a 710-nm threshold wavelength (F_2; Omega Optical, Inc., Brattleboro, VT) before being sent into a spectrograph (Oriel MS257 with an Andor V420-OE CCD camera). The specimen is piezo scanned in three dimensions with a PXY 101 CAP (piezosystem Jena, Jena, Germany) for *xy* scanning and a home-built piezo driven *z*-scanner with capacitive sensor (Queensgate NS50 nanosensor) feedback. The scanning range was 100 μm in *x*, *y*, and *z*. The dwell time per specimen position depends on the signal strength but was typically between 20 and 100 ms for the imaging of lipid vesicles. The spectral resolution is determined by the resolving power of the spectrograph of ~5 cm^{-1}. (Note that the resolution inherent in the multiplex CARS experiment is determined by the *Laser* bandwidth of 1.5 cm^{-1}.)

Laser Characteristics. Two tunable mode-locked Ti/sapphire lasers, pumped by an Nd/YVO4 laser (all from Spectra Physics, Mountain View, CA) are used for *Laser* and *Stokes* excitation. One of the Ti/sapphire lasers, the *Laser*, is a 10-ps (bandwidth

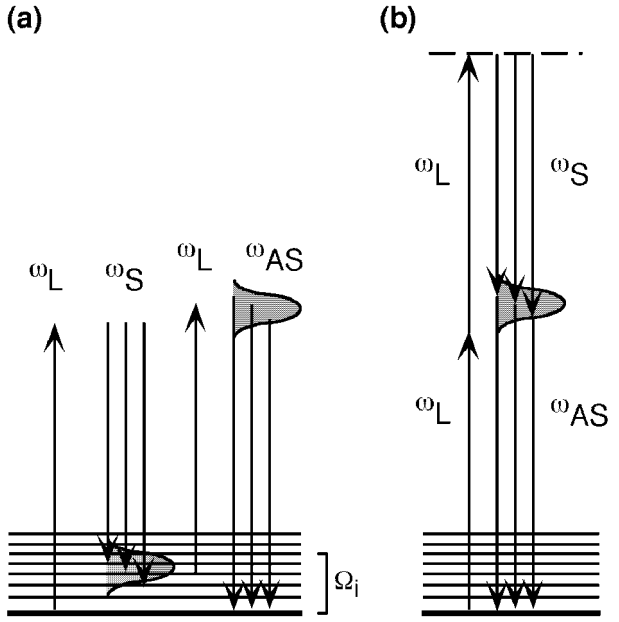

Figure 1. Energy-level diagrams for the resonant (a) and nonresonant contribution (b) to the multiplex CARS signal. The resonant contribution has a two-photon resonance with a vibrational transition (Ω_i) that is absent in the nonresonant contribution. The two contributions have the same power dependence on the input laser intensities. Also, the same phase-matching condition applies.

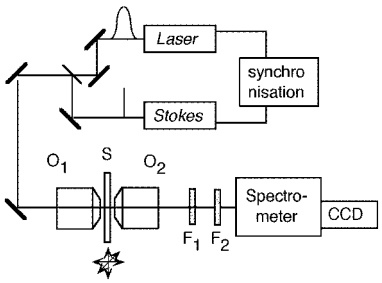

Figure 2. Schematic of the experimental setup for multiplex CARS microscopy. Symbols used: *Laser* and *Stokes*, 10 ps and 80 fs mode-locked Ti/sapphire lasers (the envelope schematically indicates the relative temporal profiles), respectively; O, microscope objective; S, sample; and F, filter. The laser pulses from the two lasers are actively synchronized in time.

of ~1.5 cm^{-1}) laser with the wavelength set at 710 nm. The other, the *Stokes*, is an ~80-fs (bandwidth of 184 cm^{-1} fwhm) laser tunable from 700 to 1000 nm. This tunability range corresponds to the "fingerprint" vibrational frequency range of 0−4000 cm^{-1}. The repetition rate of the lasers is 80 MHz, and in imaging experiments, ~100 pJ/pulse of *Laser* power and ~200 pJ/pulse of *Stokes* power is used on the sample. An interference and long-wave pass filter are used in the *Laser* and *Stokes* beam to block amplified spontaneous emission (ASE) from the lasers. The pulses of the lasers are synchronized by a "Lok-to-Clock" system (Spectra Physics, Mountain View, CA) with an additional home-built, long-term feedback system providing a timing jitter between the lasers of <1 ps. To limit possibly detrimental multiphoton absorption processes in the sample, the *Stokes* laser was stretched in time from ~80 fs to ~3 ps using a grating pair, which limits the effective bandwidth from 184 to 164 cm^{-1}.

CARS Spectrum. In a plane-wave approximation and for a nonabsorbing medium, the CARS signal is given by[15]

$$I_{\mathrm{CARS}} \propto |\chi^{(3)}|^2 I_{\mathrm{L}}^2 I_{\mathrm{S}} \operatorname{sinc}^2(\Delta\mathbf{k} \cdot d/2) \tag{1}$$

where I_i (i = L, S) is the intensity of the *Laser* and *Stokes* field respectively, d is the thickness of the scattering volume, and $\Delta\mathbf{k} = \mathbf{k}_{\mathrm{AS}} - 2\mathbf{k}_{\mathrm{L}} + \mathbf{k}_{\mathrm{S}}$ describes the phase mismatch. For a sample consisting of one or more molecular species, the CARS signal is proportional to

$$I_{\mathrm{CARS}} \propto |\sum_k N_k \chi_k^{(3)}|^2 \tag{2}$$

where N_k denotes the number of molecules of type k. The nonlinear susceptibility ($\chi^{(3)}$) for each molecular species consists of a resonant (R) and a nonresonant (NR) contribution (see Figure 1):

$$\chi^{(3)} = \chi_{\mathrm{R}}^{(3)} + \chi_{\mathrm{NR}}^{(3)} \tag{3}$$

Far away from one-photon resonances, the two-photon resonant Raman contribution to the nonlinear susceptibility can be written as

$$\chi_R^{(3)} \propto \sum_j \frac{R_j}{\delta_j - i\Gamma_j} \tag{4}$$

where R_i is a real constant containing the vibrational scattering cross section of the vibrational mode i, $\delta_i = \Omega_i - \omega_{\mathrm{L}} + \omega_{\mathrm{S}}$ denotes the detuning from the vibrational resonance Ω_i, Γ_i is the hwhm of the spontaneous Raman scattering vibrational transition, and the summation is over all vibrational resonances. It follows from these expressions that the CARS spectral line shape is given by

$$\begin{aligned} I_{\mathrm{CARS}} \propto & \sum_{k,l} N_k \chi_{k,\mathrm{NR}}^{(3)} N_l \chi_{l,\mathrm{NR}}^{(3)} \\ & + 2\sum_{k,l}\left\{ N_k N_l \chi_{k,\mathrm{NR}}^{(3)} \sum_i \frac{\delta_{li} R_{li}}{\delta_{li}^2 + \Gamma_{li}^2} \right\} \\ & + \sum_{k,l}\left\{ N_k N_l \sum_{i,j} \frac{R_{ki} R_{lj} (\delta_{ki}\delta_{lj} + \Gamma_{ki}\Gamma_{lj})}{(\delta_{ki}^2 + \Gamma_{ki}^2)(\delta_{lj}^2 + \Gamma_{lj}^2)} \right\} \end{aligned} \tag{5}$$

where the subscripts k, l are over the different molecular species and i, j are over the vibrational resonances of each molecular species. In comparison, the spontaneous Raman scattering line shape is described by the sum of the Lorentzian contributions:

$$I_{\mathrm{Raman}} \propto \sum_k \left\{ \sum_i \frac{N_k R_{ki}}{\delta_{ki}^2 + \Gamma_{ki}^2} \right\} \tag{6}$$

For the experiments considered in this contribution, the sample consists of two molecular species: lipids and water. Because the water molecules have no significant vibrational resonances within the range of the Raman frequencies of observation, we have $\chi_{\mathrm{water}}^{(3)} \cong \chi_{\mathrm{water,NR}}^{(3)}$. In addition, for low lipid concentration, $\chi_{\mathrm{lipid,R}}^{(3)} << \chi_{\mathrm{water,NR}}^{(3)}$ and the third term of eq 5 becomes negligible. It follows that the main differences between the CARS spectrum and the spontaneous Raman spectrum are the constant background (first term in eq 5) and the dispersive shape (due to the second term in eq 5) of the spectral features in CARS, in contrast to the typical Lorentzian shapes in Raman.

Spontaneous Raman Scattering. The spontaneous Raman scattering spectra of individual multi-lamellar vesicles was measured with a Raman microscope (Renishaw RM1000 system, Wotton-under-Edge, U.K.). This system provides a spectral resolution of 1 cm^{-1} and uses a 6-mW HeNe laser for excitation. A typical acquisition time for the Raman spectrum of a lipid vesicle with this instrument is 15 min.

Vesicle Preparation. 1,2-distearoyl-*sn*-glycero-3-phosphocholine (DSPC; 18:0) and 1,2-dioleoyl-*sn*-glycero-3-phosphocholine (DOPC; 18:1, 9-cis) were obtained from Avanti Polar lipids (Alabaster, AL) and used without further purification. Multi-lamellar vesicles were prepared as follows: 2 mg of dried lipid was hydrated in 1 mL of Millipore water (~2.5 mM). The mixtures were stirred for 2 min on a Vortex and then heated for 2 min above the phase-transition temperature. This process was repeated three times, resulting in multi-lamellar vesicles with a large distribution in size. The vesicles were contained in an ~50 μm compartment between two cover slips. The DSPC vesicles showed spontaneous adhesion to the glass surface. The DOPC vesicles, on the other hand, required fixation using poly-L-lysine (PLL). The morphology of the vesicles and their fixation were checked in a phase-contrast microscope.

Image Acquisition and Data Analysis. The multiplex CARS images result from a point-by-point acquisition of the CARS spectrum. The specimen is raster scanned using the piezo-driven *xyz* translators, and at each specimen position, the CARS spectrum was collected over an ~400 cm^{-1} bandwidth. The spectral data for each specimen position are subsequently fitted to the theoretical expression of the CARS signal (eq 5) for the molecular species of interest, including the intensity profile of the *Stokes* laser spectrum, which is approximated by a Gaussian shape. The Raman-specific molecular parameters (vibrational resonance frequencies, line widths, and amplitudes) can either be determined directly from the fit or determined independently from spontaneous Raman spectroscopy, which provides an internal check of the data. The only free-fitting parameters used in the fitting procedure that generates the images are the amplitude of the Gaussian spectral-intensity profile, the magnitude of the nonresonant background, and the amplitudes of the Raman spectral features.[20] Finally, the multiplex CARS microscopic image results from plotting the amplitude of one of the CARS spectral features as a function of the specimen position. Because the amplitudes of the different CARS spectral features within the detection band are highly correlated, the specific choice of the Raman mode is immaterial. The accuracy

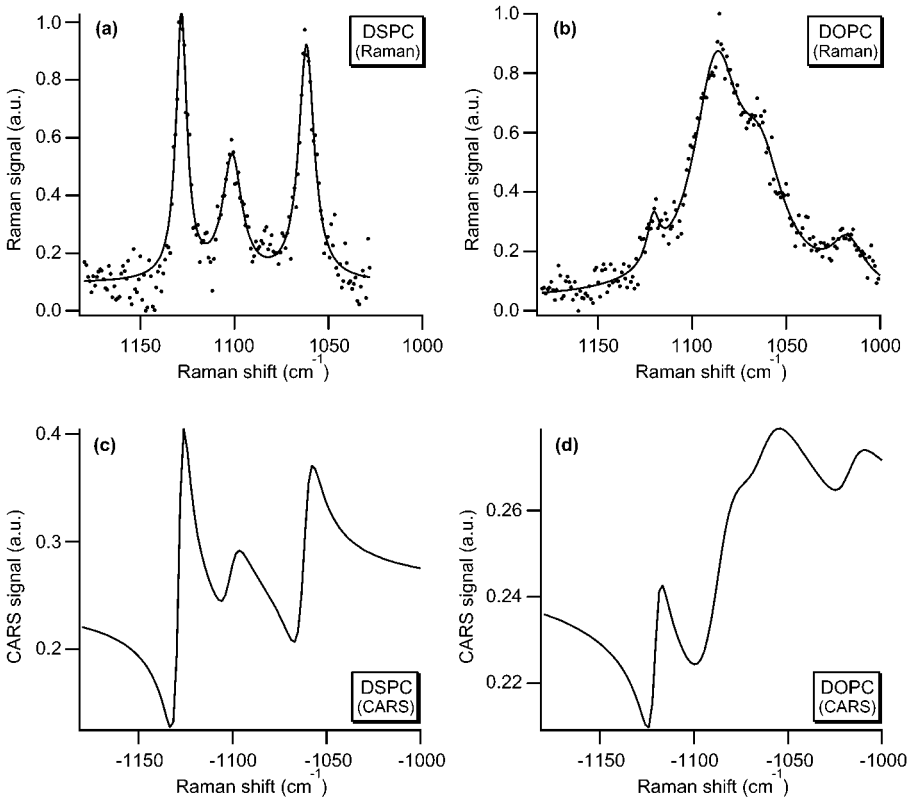

Figure 3. Spontaneous Raman spectrum of a DSPC (a) and a DOPC (b) multi-lamellar vesicle at room temperature. The solid line is the fit of the data to the sum of three (a) and four (b) Lorentzian contributions. Parameters from the fit for DSPC: $\Gamma_1 = 5.1 \pm 0.3$ cm^{-1}, $\Omega_1 = 1061.5 \pm 0.2$ cm^{-1}, $\Gamma_2 = 6.5 \pm 0.7$ cm^{-1}, $\Omega_2 = 1101 \pm 0.4$ cm^{-1}, $\Gamma_3 = 3.3 \pm 0.2$ cm^{-1}, $\Omega_3 = 1128.1 \pm 0.1$ cm^{-1}. For DOPC: $\Gamma_1 = 11.1 \pm 2.0$ cm^{-1}, $\Omega_1 = 1017.3 \pm 1.1$ cm^{-1}, $\Gamma_2 = 15.2 \pm 1.8$ cm^{-1}, $\Omega_2 = 1063.6 \pm 1.2$ cm^{-1}, $\Gamma_3 = 14.8 \pm 0.9$ cm^{-1}, $\Omega_3 = 1087.3 \pm 0.6$ cm^{-1}, $\Gamma_4 = 4.0 \pm 1.0$ cm^{-1}, $\Omega_4 = 1120.7 \pm 0.6$ cm^{-1}. Calculated CARS spectral profiles on the basis of parameters obtained from spontaneous Raman scattering from a DSPC (c) and a DOPC (d) multi-lamellar vesicle.

with which the relative amplitudes of the different Raman modes can be resolved from the CARS spectra is determined only by Poisson noise.

Results

Spontaneous Raman and CARS Spectrum. The general relation between the spontaneous Raman scattering spectrum and that obtained with CARS follows from eq 6 and 5, respectively. The Raman spectrum is characterized by the sum of the Lorentzian-shaped vibrationally resonant contributions. The strength of the signal is linearly proportional to the Raman scattering cross section and the laser intensity. The CARS spectrum, on the other hand, is proportional to the square of the sum of both the resonant and nonresonant contributions, yielding a dispersive contribution for each resonance and interference between overlapping spectral modes. At high molecular concentrations, the signal strength is proportional to the square of the number density (third term in eq 5), whereas at low concentrations, the signal is dominated by the cross term (second term in eq 5) and the dependence becomes linear.

Figure 3 shows the spontaneous Raman spectrum, taken at room temperature, of a DSPC (Figure 3a) and a DOPC multilamellar vesicle (Figure 3b). The spectra show the so-called skeletal optical mode spectral region around 1100 cm^{-1}. This region reflects the C−C skeletal stretching modes of the lipid acyl chains and permits a direct observation of gauche conformers along these acyl chains (see ref 16). For DSPC and DOPC, the phase-transition temperatures are at 54.3 and −20 °C, respectively. Below the phase-transition temperature, the lipids are in the gel phase, and the Raman spectrum in this region is dominated by three contributions, which have been assigned to an all-trans out-of-phase skeletal stretching mode (at ∼1062 cm^{-1}) and all-trans in-phase skeletal stretching modes (at ∼1100 and ∼1129 cm^{-1}).[17] The solid line in Figure 3a is the fit of the Raman signal to the sum of the three Lorentzian contributions, according to eq 6.

Upon chain melting (i.e., above the phase-transition temperature), the intensities of all the all-trans modes decrease, and the 1129 cm^{-1} feature shifts downward by ∼8 cm^{-1}. A new feature at ∼1019 cm^{-1} appears. In addition, all spectral features broaden significantly. In Figure 3b, the solid line represents the fit of the Raman signal to, in this case, the sum of the four Lorentzian contributions.

The theoretically expected CARS signal can be calculated from the spontaneous Raman scattering data using eq 5. The only free parameter in this case is the magnitude of the nonresonant background. The results are shown in Figures 3c and d for DSPC and DOPC, respectively. The magnitude of the nonresonant background ($|\chi^{(3)}_{NR}|$) was chosen to give the best agreement with the experimentally observed CARS signal (see below). The general shape of the CARS spectrum is as follows. The nonresonant background signal provides a constant contribution to the CARS signal, which is independent of the Raman shift. The purely resonant signal is identical to the spontaneous Raman signal except for the squared amplitude (R_i^2, see eq 5). Finally, the mixing of the nonresonant and resonant contributions is responsible for the typical dispersive shape of the CARS signal.

Performance of the Multiplex CARS Microscope. Theory (eq 1) predicts a square dependence of the CARS signal on the

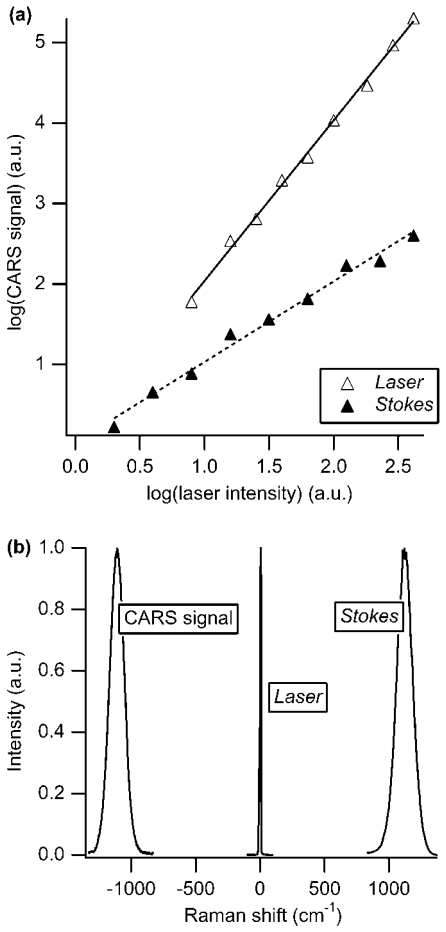

Figure 4. (a) Dependence of the CARS signal on the *Laser* (△) and *Stokes* (▲) power. The slopes of the fitted lines in the log−log plot are 2.0 ± 0.04 (△) and 1.0 ± 0.04 (▲), respectively. (b) Spectrum of the *Laser* and *Stokes* excitation and the (nonresonant) CARS signal.

Laser power and a linear dependence on the *Stokes* power, respectively. Figure 4a shows the experimental verification of this dependence. At all relevant laser powers, no deviation of the expected power dependence is observed. The spectral-intensity profiles of the *Laser*, *Stokes*, and (nonresonant) CARS signals are shown in Figure 4b. Note that the spectral resolution of the spectrometer is insufficient to resolve the *Laser* spectrum and that the CARS spectral profile mimics that of the *Stokes* laser.

The CARS spectrum observed in multiplex CARS is a product of the CARS spectrum itself and the spectral-intensity profile of the *Stokes* laser. Examples of this spectrum are shown in Figures 5a and b for a DSPC and a DOPC multi-lamellar vesicle, respectively. The wavelengths of *Laser* and *Stokes* (710 and 770 nm, respectively) are set to provide resonance with the skeletal optical mode Raman frequency range with the anti-Stokes signal centered around -1100 cm^{-1}. In the CARS spectrum, the nonresonant background, which, by definition, is Raman shift-independent, provides the approximately Gaussian-shaped contribution that reflects the *Stokes* intensity profile. On top of this background is the dispersive resonant contribution to the signal.

Figures 5c and d show the CARS signals of DSPC and DOPC, respectively, after dividing out the influence of the *Stokes* spectral-intensity profile from the signal. This is accomplished by fitting the original data to the theoretical CARS signal. For DSPC, the CARS signal can be fitted without restrictions to the fitting parameters. The fit uniquely converges to the result shown in Figure 5c, where the line-width (Γ_i) and line-position (Ω_i) parameters are in excellent agreement with the spontaneous Raman data of Figure 4. A slight discrepancy between the measured CARS spectrum and the spontaneous Raman data is found in the relative amplitudes of the various modes, where the CARS data appear to overestimate the magnitude of the -1101 cm^{-1} mode by 15% (see discussion below). For DOPC, the fitting procedure is less unambiguous. In the liquid crystalline phase, all spectral modes broaden and decrease in amplitude. In addition, low-intensity features at -1017 and -1121 cm^{-1} appear in the wings of the *Stokes* spectral-intensity profile. This combination of spectral changes makes the fit quite sensitive to the exact shape of the *Stokes* spectral profile, which only in first approximation follows a Gaussian shape. A more exact description of the spectral profile is required in this case to retrieve the Raman parameters exactly. In Figure 5d, only the amplitudes of the spectral features are used as fitting parameters, whereas the spectral positions and line widths are taken from the spontaneous Raman data.

Identification of the Thermodynamic State of Lipids in Membranes. The results of the preceding section can be used to image the thermodynamic state of multi-lamellar vesicles. Figure 6 shows a typical multiplex CARS image (an optical section) of a DSPC vesicle, where the Raman spectral signature is characteristic of a gel-phase lipid membrane. The image is generated by raster scanning in the lateral plane of the vesicle while keeping the axial position constant. For each point, a CARS spectrum is measured. After completing the acquisition, each CARS spectrum is fitted to the theoretical curve (eq 5), and the image is generated by plotting the amplitude of the -1128 cm^{-1} mode. Typical CARS spectra for the lipids and the water are shown in the insets. The latter has a nonresonant contribution only.

Figure 7 shows a multiplex CARS image with both a gel-phase DSPC vesicle and a cluster of liquid crystalline-phase DOPC vesicles within the field of view. This image is obtained within a single scan of the specimen, where the discrimination between the two types of vesicles is based only on differences in the CARS spectra obtained at each specimen position. Typical spectra, with an acquisition time of 50 ms, obtained for DSPC and DOPC are shown in the insets. The spectral data at each point were subsequently fitted to theoretical expressions for the CARS signals of a gel-phase lipid (DSPC) and a liquid crystalline-phase lipid (DOPC). The contrast in the different (artificial) color channels, blue and yellow, is based on the amplitude of the -1128 cm^{-1} mode of the gel-phase lipids and the -1087 cm^{-1} mode of the liquid crystalline-phase lipids, respectively, as derived from the fitting of the data. The faint features, which are marked by **I** and **II**, can be identified by the CARS spectral "fingerprints" as DSPC and DOPC vesicles, respectively. It should be noted that even for an experienced observer the two types of vesicles can not be discriminated on morphological features. The absence of cross talk between the DSPC and DOPC signal should be noted in particular. From all resonant CARS signals that exceed the Poisson noise of the nonresonant background signal, the identity of the lipids can be determined, without doubt, from the curve fitting.

The axial sectioning capability of multiplex CARS is demonstrated in Figure 8. This figure shows an axial scan through a DSPC vesicle. Multiplex CARS spectra are taken at 250-nm axial intervals. The CARS spectra are fitted to the theoretical expression, and the amplitude of the -1128 cm^{-1} mode is shown as a function of the axial position. The scan clearly cuts through the two (multi-lamellar) walls of the vesicle,

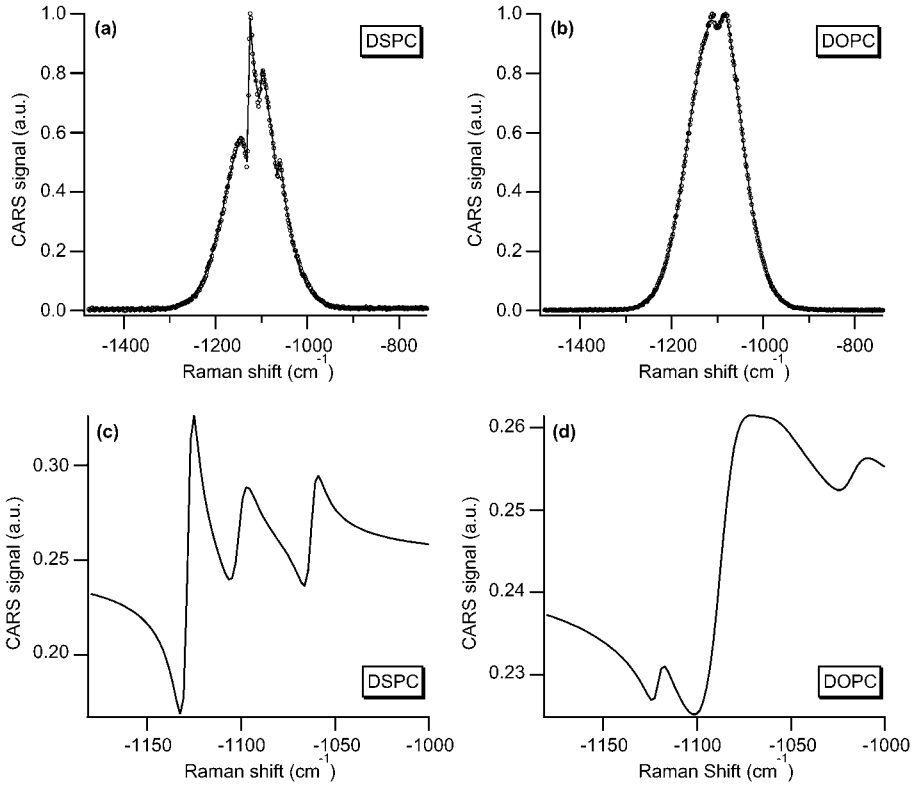

Figure 5. (a) CARS spectrum of a DSPC multi-lamellar vesicle at room temperature. The solid line is the fit of the data to eq 5, including a Gaussian *Stokes* spectral-intensity profile. The parameters from the fit are $\Gamma_1 = 3.7 \pm 0.3$ cm^{-1}, $\Omega_1 = -1061.6 \pm 0.2$ cm^{-1}, $\Gamma_2 = 5.2 \pm 0.3$ cm^{-1}, $\Omega_2 = -1101.1 \pm 0.1$ cm^{-1}, $\Gamma_3 = 3.26 \pm 0.06$ cm^{-1}, and $\Omega_3 = -1128.2 \pm 0.1$ cm^{-1}. (b) CARS spectrum of a DOPC multi-lamellar vesicle at room temperature. The solid line is the fit to the data, as in (a), with only the amplitudes of the spectral features as free-fitting parameters and all other parameters taken from the spontaneous Raman data. CARS spectral profile of the DSPC (c) and DOPC (d) vesicle after eliminating the *Stokes* spectral-intensity profile.

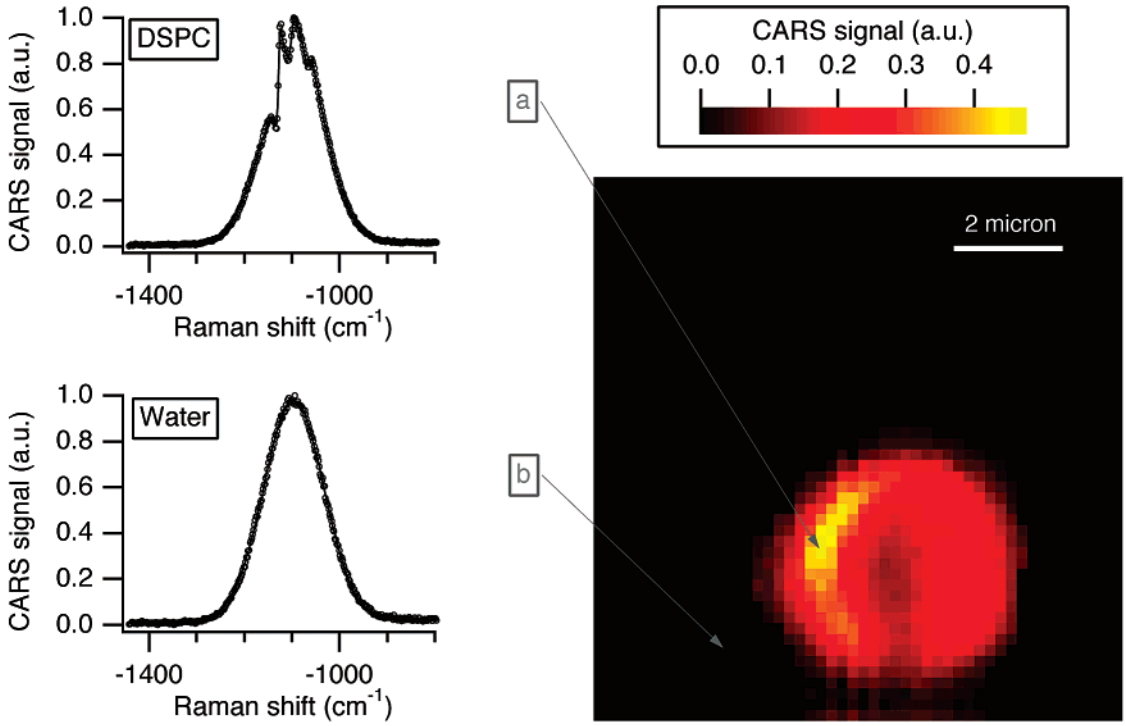

Figure 6. Multiplex CARS image of a DSPC multi-lamellar vesicle, with the contrast based on the amplitude of the -1128 cm^{-1} mode. The acquisition time per pixel is 200 ms, and the image is 50 × 50 pixels. The scale bar corresponds to 2 μm. The insets show the CARS spectrum of the lipids (a) and the surrounding water (b). The solid line represents the fit of the data to a theoretical expression based on eq 5.

with a minimum in the center of the vesicle. From a number of such axial scans, a rough estimate of the axial resolution (~1 μm) attained from this technique can be inferred. This resolution is in good agreement with the results published earlier.[4,6] The lateral resolution under these conditions can be estimated from earlier work[4,6] to be ~300 nm.

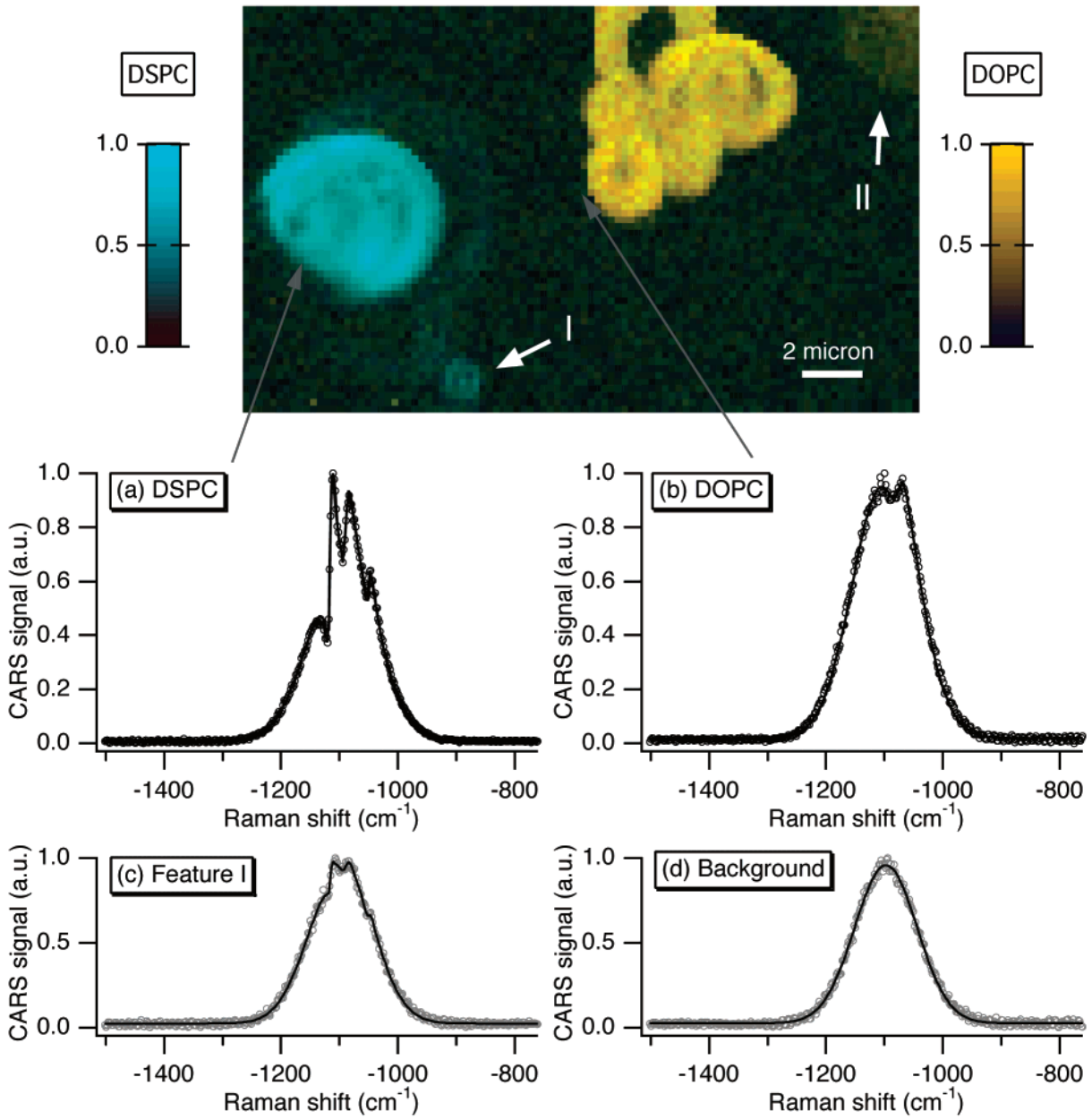

Figure 7. Multiplex CARS image of both a DSPC and a DOPC vesicle, which have been discriminated on the basis of their CARS spectrum in the skeletal optical mode region. The image is 100 × 60 pixels, with a 50-ms acquisition time per pixel. The scale bar corresponds to 2 μm. The data were subsequently fitted to theoretical expressions for the CARS signals of a gel-phase lipid (DSPC) and a liquid crystalline-phase lipid (DOPC). The contrast of the DSPC -1128 cm^{-1} Raman mode is plotted in blue, whereas the contrast of the DOPC -1087 cm^{-1} mode is plotted in yellow (color bars shown). The graphs show typical multiplex CARS spectra of DSPC (a) and DOPC (b). Graph (c) shows the CARS spectrum of the faint feature marked by **I**, which can be identified as DSPC and is readily discriminated from the (water) background shown in graph (d).

Discussion

Multiplex CARS, in particular, provides information over the full skeletal optical mode spectral range simultaneously, without requiring additional tuning of the lasers, which makes this technique insensitive to signal-strength fluctuations that are laser induced (e.g., power fluctuation, timing jitter between two lasers, etc.). In addition, the significant bandwidth of the detected CARS signal enables a multiparameter internal validation of the data. For instance, we checked whether a consistent response is obtained over the entire vesicle by plotting the ratio between the amplitudes of different spectral features as a function of spatial position. This procedure yields an identical image to that obtained when using the amplitude of a single feature only. Also, the extended detected spectral range of the CARS signal permits a consistency check of the experimental data with results obtained independently with spontaneous Raman scattering.

Signal-to-Noise. The accuracy with which the relative amplitudes of the different modes within the detection band can be resolved is determined by two factors: (i) the Poisson noise on the signal and (ii) the accuracy with which the spectral-intensity profile of the *Stokes* laser is known, which becomes increasingly important, as was shown for the DOPC vesicles, for relatively broad spectral features that are positioned in the wings of the spectral profile. For the gel-phase spectrum of DSPC, which has significantly narrower line widths, the relative amplitudes of the three spectral features can be determined more accurately. In this case, the amplitude of the -1101 cm^{-1} feature is slightly (15%) but significantly overestimated in the CARS data in comparison to the spontaneous Raman scattering data.

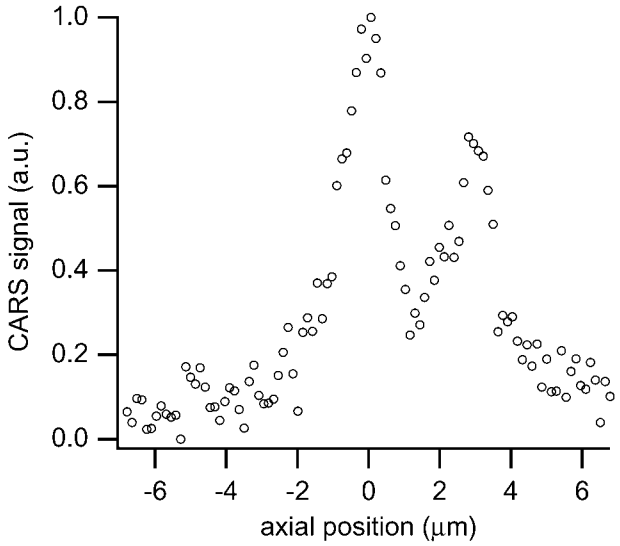

Figure 8. Axial scan through a DSPC multi-lamellar vesicle. Plotted are the amplitudes of the −1128 cm^{-1} Raman mode. Data were taken at 250-nm axial intervals with a 100-ms integration time per position. The maximum features correspond to the situation where the microscope focus coincides with one of the multi-lamellar lipid membrane walls of the vesicle, whereas the dip between features corresponds to the center of the vesicle, where the signal is dominated by the nonresonant water signal.

A possible explanation for this observation may be a slight heating of the sample in CARS. From the literature,[18] it is known that when the temperature is significantly below the phase-transition temperature the relative amplitudes of the vibrational modes in the Raman spectrum change, starting with a relative increase of the 1101 cm^{-1} feature, which is followed by further amplitude changes and spectral shifts when proceeding through the phase transition. Even if there is some local heating, the information from the full CARS spectrum, provided by multiplex CARS, enables unambiguous identification of a predominantly gel-phase lipid vesicle.

The data analysis procedure followed here yields CARS spectral amplitudes that are independent of the *Laser* or *Stokes* intensity. Thus, brighter areas in the images can explicitly be assigned to a higher local lipid number density. This internal normalization calibration of multiplex CARS renders it a robust imaging technique.

Chemical Imaging. In this article, we have selected for a first demonstration of multiplex CARS microscopy the identification of the thermodynamic state of lipid vesicles and, in particular, the response in the skeletal optical mode region of the vibrational spectrum. Of course, various other spectral regions can be used. For instance, the C−H stretching-mode region of hydrocarbon chains (2800−3100 cm^{-1}) can provide similar information about the physical state of the membrane. The headgroup region (700−1300 cm^{-1}) can be used to monitor the hydration state of the lipids, among other parameters. Also, rather than focusing on the physical state of the membrane, multiplex CARS can be used for chemical identification. For the DSPC and DOPC vesicles considered here, the unsaturation of DOPC has a pronounced spectral feature at ∼1665 cm^{-1}, which can readily be used to discriminate between DSPC and DOPC. Finally, one can consider the use of a combination of spectral bands, with tuning of the *Stokes* laser between or the use of multiple lasers, for more advanced types of identification.

Application of CARS microscopy to more complicated systems such as whole cells is possible, as has been demonstrated by Xie and co-workers.[3,7] Clearly, the analysis of the data in this case becomes more complex because a large number of different molecules contribute to the signal. The technique profits, however, from the small volume that is probed at any time because of the nonlinearity of the process. Multiplex CARS imaging will be especially useful in this case in permitting the identification of specific features on the basis of the full CARS spectrum obtained at each image position. It should be noted that spontaneous Raman (micro)spectroscopy has already been shown to be a powerful tool in whole-cell studies.[19]

Whereas in this article a full curve fitting of the experimental data to the theoretical prediction has been used, more rapid approaches to data processing, such as methods based on templates, can be contemplated.

Conclusions

Multiplex CARS microscopy enables the rapid acquisition of high-resolution microscopic images, with a contrast based on the parameters (line width, position, and/or amplitude) of one or more vibrational spectral features. This possibility arises from the simultaneous acquisition of a significant part of the vibrational spectrum. Because of the absence of absorption, no fading of contrast occurs. As a first demonstration, we applied the technique to the imaging of multi-lamellar vesicles. A further increase in sensitivity is required to apply multiplex CARS microscopy to uni-lamellar model membrane systems that are generally more appropriate to elucidate biophysical phenomena. Novel methods to increase the sensitivity of the technique to this level of investigation are currently being developed. This increased sensitivity will permit full utilization of the unique potential of this technique to probe the physical and chemical states of biological systems with high spatial 3-D resolution without the use of foreign labels or additives.

Acknowledgment. We thank N. Nastase and S. Wurpel for the preparation of the lipid vesicles and for the acquisition of the spontaneous Raman spectral data and Professor Brakenhoff for stimulating discussions and the critical reading of the manuscript. This research was financially supported, in part, by the Stichting voor Fundamenteel Onderzoek der Materie (FOM), The Netherlands, under grant no. 94RG02 and by the Stichting Technische Wetenschappen (STW), The Netherlands, under grant no. ABI.4929.

References and Notes

(1) Puppels, G. J.; de Mul, F. F. M.; Otto, C.; Greve, J.; Robert-Nicoud, M.; Arndt-Jovin, D. J.; Jovin, T. M. *Nature* **1990**, *347*, 301−303.

(2) Duncan, M. D.; Reijntjes, J.; Manuccia, T. J. *Opt. Lett.* **1982**, *7*, 350−352.

(3) Zumbusch, A.; Holtom, G. R.; Xie, X. S. *Phys. Rev. Lett.* **1999**, *82*, 4142−4145.

(4) Müller, M.; Squier, J.; de Lange, C. A.; Brakenhoff, G. J. *J. Microsc.* **2000**, *197*, 150−158.

(5) Potma, E. O.; de Boeij, W. P.; van Haastert, P. J. M.; Wiersma, D. A. *Proc. Natl. Acad. of Sci. U.S.A.* **2001**, *98*, 1577−1582.

(6) Cheng, J.; Volkmer, A.; Book, L. D.; Xie, X. S. *Journal of Physical Chemistry B* **2001**, *105*, 1277−1280.

(7) Volkmer, A.; Cheng, J.; Xie, X. S. *Phys. Rev. Lett.* **2001**, *87*, 23901−23904.

(8) Tahara, T.; Toleutaev, B.; Hamaguchi, H. *J. Chem. Phys.* **1994**, *100*, 786−796.

(9) Otto, C.; Voroshilov, A.; Kruglik, S. G.; Greve, J. *J. Raman Spectrosc.* **2001**, *32*, 495−501.

(10) Simons, K.; Ikonen, E. *Nature* **1997**, *387*, 569−572.

(11) Hooper, N. M. *Mol. Membr. Biol.* **1999**, *16*, 145−156.

(12) Jacobson, K.; Dietrich, C. *Trends Cell Biol.* **1999**, *9*, 87−91.

(13) Brown, D. A.; London, E. *J. Membr. Biol.* **1998**, *164*, 103−114.

(14) Dietrich, C.; Bagatolli, L. A.; Volovyk, Z. N.; Thompson, N. L.; Levi, M.; Jacobson, K.; Gratton, E. *Biophys. J.* **2001**, *80*, 1417−1428.

(15) Eesley, G. L. *Coherent Raman Spectroscopy*; Pergamon Press: New York, 1981.

(16) Gaber, B. P.; Peticolas, W. L. *Biochim. Biophys. Acta* **1977**, *465*, 260−274.

(17) Batenjany, M. M.; Wang, Z.; Huang, C.; Levin, I. W. *Biochim. Biophys. Acta* **1994**, *1192*, 205−214.

(18) Levin, I. W. Vibrational Spectroscopy of Membrane Assemblies. In *Advances in Infrared and Raman Spectroscopy*; Clark, R. J. H., Hester, R. E., Eds.; Wiley & Sons: New York, 1984; Vol. 11, pp 1−48.

(19) Puppels, G. J.; Greve, J. Whole Cell Studies and Tissue Characterization by Raman Spectroscopy. In *Biochemical Applications of Spectroscopy*; Clark, R. J. H., Hester, R. E., Eds.; Wiley & Sons: New York, 1996; pp 1−47.

(20) Note that the amplitude of the Stokes spectral-intensity profile, the magnitude of the nonresonant background, and the amplitude of the Raman spectral features are not independent parameters. In fact, for every change in the value of the amplitude of the Stokes spectral-intensity profile, compensating values for the nonresonant background and spectral line amplitudes can be found that provide the same quality of fit of the experimental data to the theoretical expression.